RSC Advances

ROYAL SOCIETY OF CHEMISTRY

www.rsc.org/advances

RSC Advance

ARTICLE

Synthesis and Photocatalytic Activity of N-$K_2Ti_4O_9$/UiO-66 Composites

Sunfeng Li, Xing Wang, Qi Chen, Qinqin He, Mengmeng Lv, Xueting Liu*, JianpingLv, and Fengyu Wei*

Received 00th January 20xx,
Accepted 00th January 20xx

DOI: 10.1039/x0xx00000x

www.rsc.org/

N-$K_2Ti_4O_9$/UiO-66 composites synthesized by a facile solvothermal method possess a hierarchical core-shell structure with UiO-66 forming the shell around the N-$K_2Ti_4O_9$ core. Photocatalytic activity of N-$K_2Ti_4O_9$, UiO-66 and the composites were investigated by the degradation of rhodamine B (RhB) under visible light irradiation. The synergistic effect induced by compounding was quantitatively evaluated by the proposed synergistic factor. The results show that N-$K_2Ti_4O_9$/UiO-66 composites exhibit higher photocatalytic activity as compared with the pure materials, and this is due to the high adsorption capacity of UiO-66 and the compounding induced higher separation efficiency of photogenerated electron-hole pairs. In particular, when the molar ratio of N-$K_2Ti_4O_9$ to $ZrCl_4$ is 3:7, the composite exhibits the highest photocatalytic activity, and the synergistic factor is 4.90.

Introduction

The use of solar energy and semiconductor catalysts for photocatalytic degradation of organic pollutants in water and for photocatalytic production of hydrogen through water splitting has been intensively investigated as an emerging renewable technology [1-4].

$K_2Ti_4O_9$ has been studied as a photocatalyst under UV irradiation, however, its band-gap is ca. 3.2-3.4 eV [5]. Therefore, it is of great interest to reduce the band-gap of $K_2Ti_4O_9$ in order to widen the practical applications of $K_2Ti_4O_9$ related materials via taking advantage of visible light in solar energy. Doping of N element into $K_2Ti_4O_9$ (entitled "N-$K_2Ti_4O_9$") is a common method of reducing the band-gap [6, 7].

In recent years, numerous researches have been focused on metal-organic frameworks (MOFs) materials, which are made up of metal clusters linked to each other by organic ligands [8-12]. Because of their high specific surface area and uniform but tunable pore size, the MOFs are considered as potential candidates for adsorption [13], storage [14-16], and health care applications [17]. Cavka et al. was first to synthesize a zirconium(IV)-based MOF (UiO-66) with exceptional stability [18].A recently discovered UiO-66 cornerstone is based on a $Zr_6O_4(OH)_4$ octahedron, forming lattices by 12-fold connection through a 1,4-benzene-dicarboxylate (bdc) linker [19-21]. Hence, the UiO-66 framework is quite robust, and is exceedingly open to isoreticular functionalization without losing its high hydrothermal and chemical stability. The work of the group at Valencia has shown that UiO-66 exhibits photocatalytic activity for hydrogen generation in methanol or water/methanol upon irradiation at wavelengths longer than 300 nm [22], and represents a good candidate for the development of more efficient MOF-based water-splitting materials.

In this paper, owing to the high specific surface area of UiO-66 and superior electron mobility of N-$K_2Ti_4O_9$, numerous efforts have been made to combine UiO-66 with N-$K_2Ti_4O_9$ to enhance the photocatalytic activity. We find that the N-$K_2Ti_4O_9$/UiO-66 composites exhibit much higher photocatalytic activity than both of pure N-$K_2Ti_4O_9$ and pure UiO-66. However, there is limited knowledge available about the synergistic action of the N-$K_2Ti_4O_9$/UiO-66 composites. The purpose of this study is to investigate the synergistic effect of N-$K_2Ti_4O_9$/UiO-66 composites on photodegradation of Rhodamine B (RhB), and the synergistic effect was quantitatively evaluated by the proposed synergistic factor.

Experimental

2.1. Synthesis of N-$K_2Ti_4O_9$/UiO-66 Composites

All the reagents used in our experiments were supplied by Sinopharm Chemical Reagent Co., Ltd. except P25, which is from Degussa Co., Ltd. The reagents were used as received without further purification. $K_2Ti_4O_9$ was synthesized according to the method described by Allen and coworkers [23], with N-$K_2Ti_4O_9$ prepared as described previously [24].

The N-$K_2Ti_4O_9$/UiO-66 composites were synthesized as UiO-66 with differing in N-$K_2Ti_4O_9$/$ZrCl_4$ ratio [20]. A typical method for preparing the composite is as follows: $ZrCl_4$ (0.192g), 1,4-benzenedicarboxylic acid (0.113g) and benzoic acid (1.767g) were dissolved in 83 mL DMF. Then N-$K_2Ti_4O_9$ (0.151g) was added into the solution with ultrasonic vibration for 30 min, and the mixture was transferred to a stainless steel teflon-lined autoclave of 100 mL capacity and then maintained at 393K for 24h. After this time, the autoclave was naturally cooled to room temperature. Finally the composites were filtered out, washed with $CHCl_3$, and dried at room temperature under reduced pressure. The as-prepared composite was entitled N-$K_2Ti_4O_9$/$ZrCl_4$(3:7) where the molar ratio of N-$K_2Ti_4O_9$ to

School of Chemistry and Chemical Engineering, Hefei University of Technology, Anhui Key Laboratory of Controllable Chemical Reaction & Material Chemical Engineering, Hefei 230009, China
*To whom correspondence should be addressed. Tel.: +86-551-62901458; Fax: +86-551-62901450. E-mail: wmlxt@163.com，weifyliuj@163.com

$ZrCl_4$ is 3:7. For other composites, when the molar ratio of N-$K_2Ti_4O_9$ to $ZrCl_4$ is *x:y*, the composite was named as N-$K_2Ti_4O_9$/$ZrCl_4$(*x:y*).

2.2. Characterization

X-ray diffraction (XRD) patterns of the samples were determined in the range of 2θ=4°-50° by step scanning on a Rigaku D/max-2500V X-ray diffractometer using Cu-Kα (λ=0.154nm) radiation.The morphological analysis of the samples was studied using a JEM-2100F field emission transmission electron microscopy (FETEM) equipped with an energy-dispersive X-ray spectrometer (EDS). UV-vis spectra were recorded on a DUV-3700 spectrometer. The valence band X-ray photoelectron spectroscopy (XPS) was conducted using an ESCALAB250 spectrometer. Photoluminescence (PL) emission spectra were measured on a PL measurement system (FluorologTau-3) with the excitation wavelength of 320nm. N_2 adsorption-desorption (BET) were performed on a Tristar II 3020M surface area and porosity analyzer. Thermogravimetric analysis (TGA) of samples was carried out on a Perkin-Elmer Diamond TG thermal analyzer at a rate of 30 K/min. The transient photocurrent responses were measured on an electrochemical system (CHI-660D).

2.3. Photocatalytic Experiments

The photocatalytic degradation of RhB was measured at ambient pressure and 298K in a set of home-made photochemical reaction equipment. The light source was a PHILIPS 12W Energy-saving lamp (λ< 380 nm was filtered out by a cut off filter).20mg of photocatalyst was added into 100 mL RhB (5mg/L) aqueous solution. Before irradiation, the suspension was continuously stirred for 24 h in the dark in order to reach the adsorption-desorption equilibrium between RhB and the photocatalyst. The supernatant liquid was obtained through filtration by 0.22μm filter, and examined using a Shimadzu UV-240 spectrophotometer. For comparison, the photocatalytic activities of UiO-66 and N-$K_2Ti_4O_9$ were also tested under the identical condition.

Results and discussion

3.1. Photocatalysts Characterization

The FETEM images were collected for pure UiO-66 and N-$K_2Ti_4O_9$, as shown in Figure 1a and Figure 1b, respectively. Pure UiO-66 are shown as discoid nanoparticles with the size in the range of 20-50nm, and obviously aggregate. In contrast, pure N-$K_2Ti_4O_9$ in Figure 1b present the nanofibers with the diameter between 100 nm and 350 nm, and the length at a few micrometers. For N-$K_2Ti_4O_9$/$ZrCl_4$(3:7), the FETEM image (Figure 1c) shows that the N-$K_2Ti_4O_9$ nanofiber was covered with the UiO-66 nanoparticles. The EDS spectra of N-$K_2Ti_4O_9$/$ZrCl_4$(3:7) in Figure 1d indicate that K, Ti, Zr, and O elements are the main chemical components present in the composite. The approximate K/Ti atom ratio of 1:2 agrees well with the theoretical value for N-$K_2Ti_4O_9$. The Zr/O atom ratio in UiO-66 and K/O atom ratio in N-$K_2Ti_4O_9$ are 6:32 and 2:9 respectively. The aggregate value of the O element based on Zr and K element contents is 65.68%, and is basically in agreement with the EDS result. It can be seen from Figure 1e to Figure 1h that UiO-66 and N-$K_2Ti_4O_9$ were not uniformly distributed in the composite. K and Ti distributions by EDS mapping (Figure 1e and 1f) show that N-$K_2Ti_4O_9$ is a core rod in the composite. However, most of Zr ions were distributed around the core rod (Figure 1g). These confirm that the composite possesses a hierarchical core-shell structure with UiO-66 forming the shell around the N-$K_2Ti_4O_9$ core.

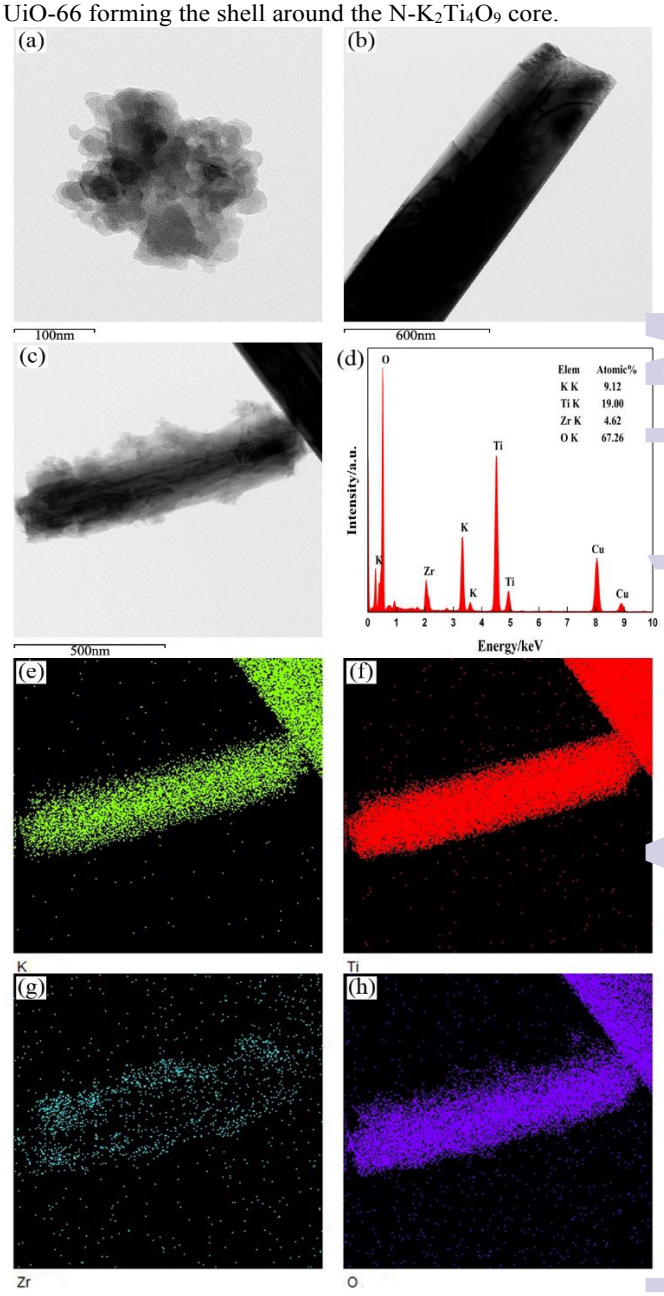

Figure 1.FETEM images of (a) UiO-66, (b) N-$K_2Ti_4O_9$, (c) N-$K_2Ti_4O_9$/$ZrCl_4$(3:7); (d) the EDS of N-$K_2Ti_4O_9$/$ZrCl_4$(3:7); (e) K, (f) Ti, (g) Zr, and (h) O distribution by EDS mapping.

The XRD patterns of UiO-66, N-$K_2Ti_4O_9$ and N-$K_2Ti_4O_9$/$ZrCl_4$(3:7) are shown in Figure 2a, which are in accordance with the one reported in the literature [18]. By comparing the XRD patterns of N-$K_2Ti_4O_9$/$ZrCl_4$(3:7) with those of the precursors UiO-66 and N-$K_2Ti_4O_9$, it can be seen that the composite displays the characteristic peaks of both UiO-66 and N-$K_2Ti_4O_9$, and the intensity and location of peak

also changes a little. That is to say, the composite is not a simple physical mixture, and there exists certain interface interactions between UiO-66 and N-$K_2Ti_4O_9$.

To determine the UiO-66 content in the composites, the thermogravimetric analyses (TGA) for UiO-66 and composites were studied. As shown in Figure 2b, all curves show three steps: the first step is assigned to the loss of physically adsorbed water molecules during heating to 100°C; the second in range of 100-450°C is related to the removal of the residual hydroxyl groups on the surface of UiO-66; the third above 450°C is ascribed to the decomposition of the linkers [25]. However, UiO-66 and the composites have differed on the residual mass. As there is no change of N-$K_2Ti_4O_9$ in the process of TGA, the UiO-66 and N-$K_2Ti_4O_9$ contents with mass percent in the composites were determined by the following equations:

$$m_{N\text{-}K_2Ti_4O_9/ZrCl_4(x:y)} \times r_{N\text{-}K_2Ti_4O_9/ZrCl_4(x:y)} = m_{N\text{-}K_2Ti_4O_9} \times r_{N\text{-}K_2Ti_4O_9} + m_{UiO\text{-}66} \times r_{UiO\text{-}66} \quad \ldots (1)$$

$$m_{N\text{-}K_2Ti_4O_9/ZrCl_4(x:y)} = m_{N\text{-}K_2Ti_4O_9} + m_{UiO\text{-}66} \quad \ldots\ldots (2)$$

Where $m_{N\text{-}K_2Ti_4O_9/ZrCl_4(x:y)}$, $m_{N\text{-}K_2Ti_4O_9}$, $m_{UiO\text{-}66}$, $r_{N\text{-}K_2Ti_4O_9/ZrCl_4(x:y)}$, $r_{N\text{-}K_2Ti_4O_9}$ and $r_{UiO\text{-}66}$ are the mass and residual mass fraction (%) of N-$K_2Ti_4O_9$/$ZrCl_4$(*x*:*y*), N-$K_2Ti_4O_9$ and UiO-66 (Table 1). As shown, the N-$K_2Ti_4O_9$ content increases with the residual mass fraction increasing in the composites.

Table 1. The N-$K_2Ti_4O_9$ and UiO-66 contents in the composites

Sample	the residual mass fraction (r)/%	the UiO-66 content(*C*) /%	the N-$K_2Ti_4O_9$ content(1-*C*)/%
N-$K_2Ti_4O_9$	100	0	100
UiO-66	32.6	100	0
N-$K_2Ti_4O_9$/$ZrCl_4$(1:9)	62.9	55.1	44.9
N-$K_2Ti_4O_9$/$ZrCl_4$(2:8)	73.5	39.4	60.6
N-$K_2Ti_4O_9$/$ZrCl_4$(3:7)	80.1	29.6	70.4
N-$K_2Ti_4O_9$/$ZrCl_4$(4:6)	81.8	27.0	73.0
N-$K_2Ti_4O_9$/$ZrCl_4$(5:5)	85.7	21.2	78.8

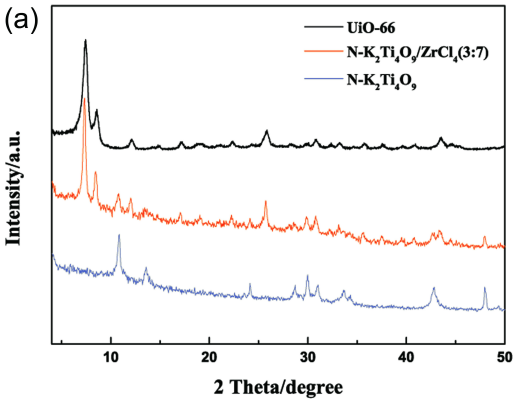

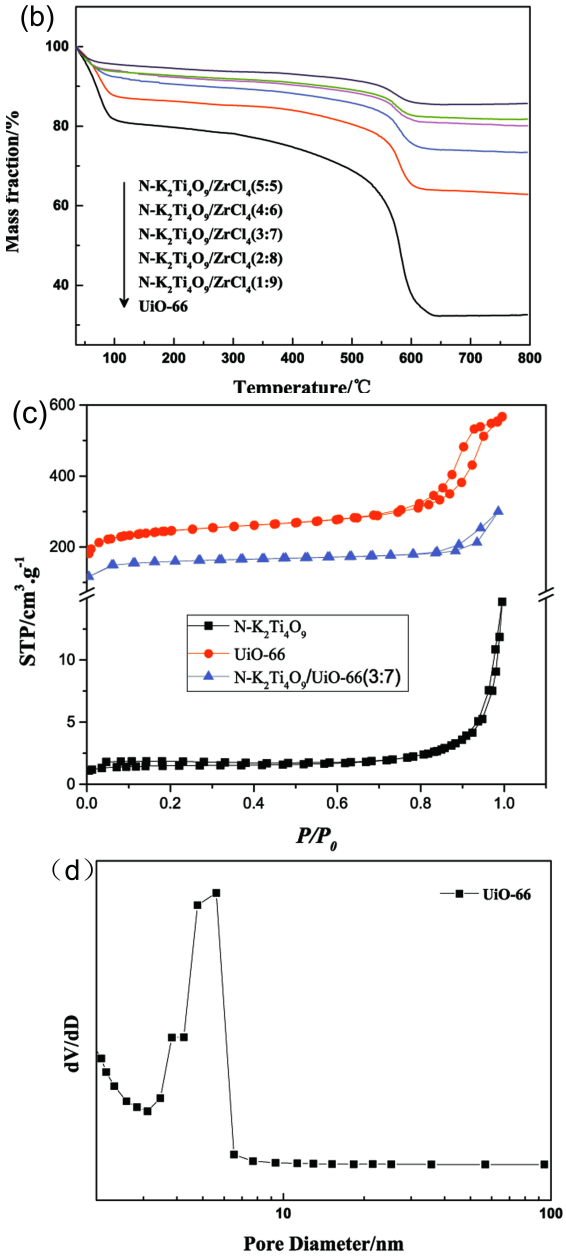

Figure **2.** (a) The XRD patterns of UiO-66, N-$K_2Ti_4O_9$ and N-$K_2Ti_4O_9$/$ZrCl_4$(3:7); (b) the TGA for UiO-66 and composites; (c) the N_2 adsorption-desorption isotherms of N-$K_2Ti_4O_9$, UiO-66 and N-$K_2Ti_4O_9$/$ZrCl_4$(3:7); (d) the BJH pore diameter distribution curve of UiO-66.

The N_2 adsorption-desorption isotherms of UiO-66, N-$K_2Ti_4O_9$ and N-$K_2Ti_4O_9$/$ZrCl_4$(3:7) are displayed in Figure 2c, and the values of BET surface area of UiO-66,N-$K_2Ti_4O_9$ and N-$K_2Ti_4O_9$/$ZrCl_4$(3:7) are 873.91 m^2/g, 4.97 m^2/g and 503.85m^2/g, respectively. The average pore size of N-$K_2Ti_4O_9$/$ZrCl_4$(3:7) is 3.186nm with its pore volume at 0.227cc/g. The N_2 isotherm of UiO-66 is categorized as type IV, as a result of a significant hysteresis loop observed in the relative pressure (*P*/*P*$_0$) range of 0.5-1.0. This property implies the presence of mesopores (2-50 nm in size) [26], which can be further verified by the Barret-Joyner-Halenda (BJH) pore size distribution curve of UiO-66 (Figure 2d). In contrast, there is no

mesopores structure in N-$K_2Ti_4O_9$ sample. When UiO-66 was loaded on the surface of N-$K_2Ti_4O_9$, the BET surface area increased, and the N_2 isotherm of N-$K_2Ti_4O_9$/$ZrCl_4$(3:7) can be categorized as type Ⅳ similar to that of UiO-66, which means the mesopores structure of N-$K_2Ti_4O_9$/$ZrCl_4$(3:7) should be brought by UiO-66.

The photoelectric properties of the composites have also been studied, and the UV-vis absorption spectra of the different samples are illustrated in Figure 3a. N-$K_2Ti_4O_9$ clearly shows a characteristic absorption of $K_2Ti_4O_9$[27] in the UV region and a new absorption shoulder at 400-500 nm (3.10eV-2.48eV) that can be attributed to the N surface plasmon resonance with the $K_2Ti_4O_9$ interband transition. The steep shape of UiO-66 shown in the UV region is due to the band-gap transition, and the prolonged absorption tail until 500 nm in the spectrum should result from the crystal defects formed during the cooling process [28]. Near the absorption band edge, the optical absorption has the following behavior:

$$\alpha h\nu = A(h\nu - E_g)^{n/2} \quad (3)$$

Where α, ν, E_g, A are absorption coefficient, light frequency, band-gap, a constant respectively, and n depends on whether

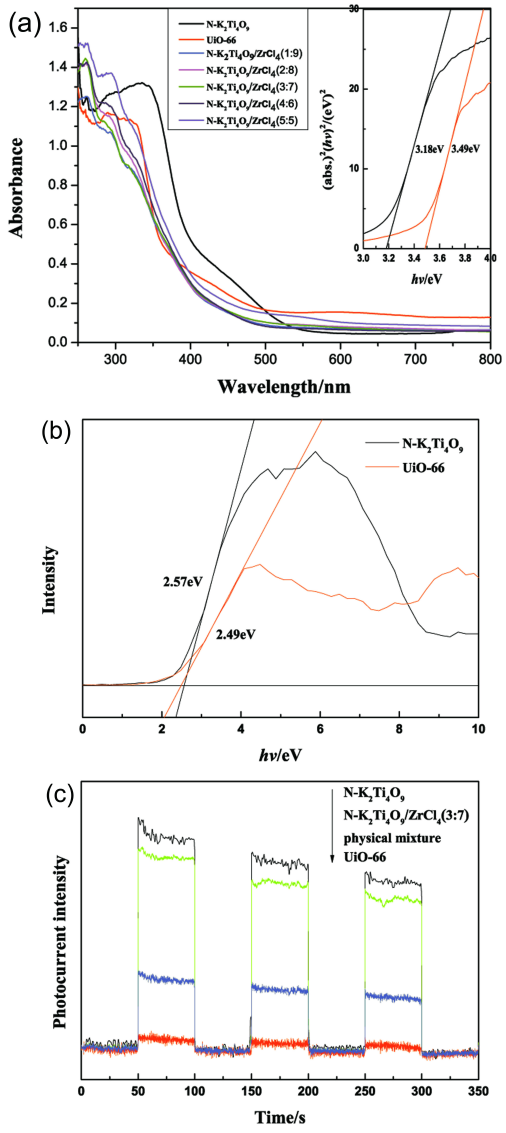

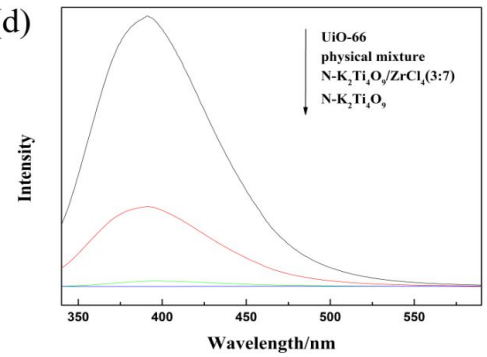

Figure 3. (a) The UV-vis absorption spectra ofUiO-66 , N-$K_2Ti_4O_9$ and N-$K_2Ti_4O_9$/$ZrCl_4$(3:7);(b) the Valence band XPS spectra of UiO-66 and N-$K_2Ti_4O_9$; (c) Photocurrent transient responses and (d) PL spectra of UiO-66, N-$K_2Ti_4O_9$, physical mixture and N-$K_2Ti_4O_9$/$ZrCl_4$(3:7)

the transition is direct (n = 1) or indirect (n = 4) [29]. For UiO-66 and N-$K_2Ti_4O_9$, the value of n is 1. The band-gaps of UiO-66 and N-$K_2Ti_4O_9$ estimated from the intercept of the tangents to the plots are 3.49 and 3.18 eV, respectively (inset in Figure 3a). As shown in Fig.3 (a), the composite photocatalysts show the similar absorbance edge to pure UiO-66, but extend the absorbance to the visible region due to the presence of N-$K_2Ti_4O_9$, and theis absorption intensity increases with increasing of N-$K_2Ti_4O_9$ content.

The valence bands of UiO-66 and N-$K_2Ti_4O_9$ were also measured by valence band XPS, as shown in Figure 3b [30]. The valence band of N-$K_2Ti_4O_9$ is at about 2.57eV, because the band-gap of N-$K_2Ti_4O_9$ is 3.18eV from the UV-vis absorption spectra, the conduction band minimum will occur at about -0.61eV. Likewise, the valence band and conduction band of UiO-66 are at about 2.49eV and -1.00eV, respectively.

The mobility of charge carriers can be understood by the transient photocurrent measurements [31, 32]. As shown in Figure 3c, via several on-off cycles of irradiation, the transient photocurrent responses of pure UiO-66, N-$K_2Ti_4O_9$ and N-$K_2Ti_4O_9$/$ZrCl_4$(3:7) were recorded. N-$K_2Ti_4O_9$ displays the highest photocurrent intensity, which means the highest migration rate and the lowest recombination rate of charge carriers. By comparison, UiO-66 exhibits the lowest photocurrent intensity. It is worth noting that the photocurrent intensity of N-$K_2Ti_4O_9$/$ZrCl_4$(3:7) is little lower than that of N-$K_2Ti_4O_9$, but much higher than that of physical mixture that consists of 29.6% UiO-66 and 70.4% N-$K_2Ti_4O_9$ (the same component as N-$K_2Ti_4O_9$/$ZrCl_4$(3:7) (Table 1)).This result shows that the compounding of UiO-66 and N-$K_2Ti_4O_9$ can inhibit the recombination of photogenerated electron-hole pairs through promoting the charge carrier transfer at the interface between UiO-66 and N-$K_2Ti_4O_9$.

Due to the direct result of the recombination of the free carriers, the photoluminescence (PL) emission spectra can be regarded as an effective approach to understand the separation efficiency of photogenerated electron-hole pairs [33, 34]. The photoluminescence (PL) emission spectra for samples under excitation at 320 nm were examined in the wavelength range of 340-590 nm as shown in Figure 3d. Interestingly, by comparing Figure 3c with Figure 3d, one can see that the order of the PL

spectra intensities of UiO-66, N-$K_2Ti_4O_9$, N-$K_2Ti_4O_9$/$ZrCl_4$(3:7) and physical mixture is contrary to that of their photocurrents.

3.2. Adsorption Activity of N-$K_2Ti_4O_9$, UiO-66 and the Composites.

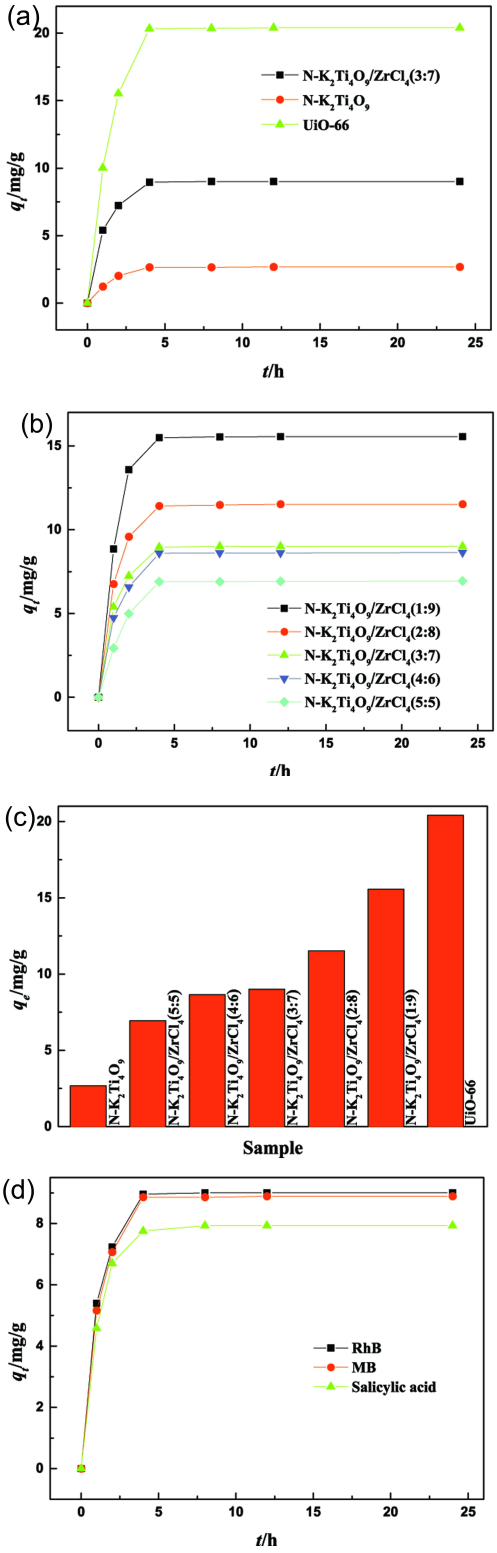

Figure **4.** (a) Adsorption capacity of RhB onto N-$K_2Ti_4O_9$, UiO-66 and N-$K_2Ti_4O_9$/$ZrCl_4$(3:7); (b) Adsorption capacity of RhB onto the composites with different molar ratios of N-$K_2Ti_4O_9$ to $ZrCl_4$; (c) The q_e of RhB onto N-$K_2Ti_4O_9$, UiO-66 and the composites; (d) Adsorption capacity of RhB, MB and salicylic acid onto N-$K_2Ti_4O_9$/$ZrCl_4$(3:7)

N-$K_2Ti_4O_9$ displays low adsorption capacity of RhB in contrast with UiO-66 (Figure 4a). This is due to the big BET surface area and the mesopores structure of UiO-66. Furthermore, the adsorption of organic dyes onto metal-organic frameworks, for instance, UiO-66, has a great advantage as compared with that onto inorganic metal oxides such as N-$K_2Ti_4O_9$, because there exists various interactions like pi-pi stacking, hydrogen bonding, etc., between aromatic rings of RhB and UiO-66. As shown in Figure 4c, the adsorption activity of composites is between those of N-$K_2Ti_4O_9$ and UiO-66, and increases with the UiO-66 content increasing. Meanwhile, the adsorption activities of composites to different organic pollutants are very similar (Figure 4d). Thus, loading UiO-66 on the N-$K_2Ti_4O_9$ surface facilitates the transfer of RhB from solution to the composites surface, benefiting heterogeneous reactions.

3.3. Photocatalytic Activity of UiO-66, N-$K_2Ti_4O_9$ and the Composites

The photocatalytic activities of UiO-66, N-$K_2Ti_4O_9$ and the composites were evaluated using the degradation of RhB under visible light irradiation. Owing to small BET surface area of N-$K_2Ti_4O_9$ and poor separation efficiency of photogenerated electron-hole pairs of UiO-66, both UiO-66 and N-$K_2Ti_4O_9$ show low photocatalytic activity before compounding, as shown in Figure 5a. Meanwhile, the photocatalytic activity of P25 (with the same weight as other samples and the BET surface area of 50m^2/g) was also studied as a criterion, and was little higher than that of N-$K_2Ti_4O_9$ but lower than that of UiO-66. In contrast, the N-$K_2Ti_4O_9$/$ZrCl_4$(3:7) composite exhibits much better visible light photocatalytic activity than P25. This may be due to the result of the synergistic effect of the compounding of UiO-66 and N-$K_2Ti_4O_9$. In particular, the compounding enhanced the separation efficiency of photogenerated electron-hole pairs as evidenced by the PL spectra. Meanwhile, the big BET surface area of UiO-66 can favor the transfer of RhB from solution to the photocatalyst surface, benefiting heterogeneous reactions.

The photocatalytic activities of N-$K_2Ti_4O_9$/$ZrCl_4$ composites with different ratios of N-$K_2Ti_4O_9$ to $ZrCl_4$ were also studied in detail. It can be seen that the N-$K_2Ti_4O_9$/$ZrCl_4$ ratio of 3:7 is the optimum value to achieve high photodegradation activity (Figure 5b). The pseudo-first-order kinetics can simulate well the photocatalytic reaction process, and the reaction constant fitted (K) is 0.295 h^{-1} for N-$K_2Ti_4O_9$/$ZrCl_4$(3:7), whereas for N-$K_2Ti_4O_9$ under the same photocatalytic conditions, it is only 0.0351 h^{-1}. Although there are numerous literature to study the synergistic effect of composite photocatalytic systems, there is still rare literature to present a quantitative criterion to evaluate the synergistic effect. We think that synergistic effect comes from the positive interactions between the pure materials composing the composite, and there exists no synergistic effect for physical mixture, because there are no obvious interactions among the components in the physical mixture. On the other hand, photocatalytic reaction constant K can describe well the photocatalytic reaction kinetics. In order to evaluate

quantitatively the synergistic effect, equation 5 was proposed[35], in which numerator is photocatalytic reaction constant of the composite, and denominator stands for the average photocatalytic reaction constant of the physical mixture having the same component ratio as the composite of numerator.

$$SF = \frac{K_{N\text{-}K_2Ti_4O_9/ZrCl_4(x:y)}}{K_{N\text{-}K_2Ti_4O_9} \times (1-C) + K_{UiO\text{-}66} \times C} \quad \text{..... (5)}$$

where $K_{N\text{-}K_2Ti_4O_9/ZrCl_4(x:y)}$, $K_{N\text{-}K_2Ti_4O_9}$, $K_{UiO\text{-}66}$ are the photocatalytic reaction constants of N-$K_2Ti_4O_9$/$ZrCl_4$(*x*:*y*), N-$K_2Ti_4O_9$ and UiO-66, respectively and *C* is the content of UiO-66 (Table 1). As shown in equation 5, if SF is bigger than 1, it means there exists enhanced effect derived from the interface interactions of components in the composite as compared with the physical mixture. The synergistic factors of composites are all greater than 1. In particular, for N-$K_2Ti_4O_9$/$ZrCl_4$(3:7), the synergistic factor is 4.90, the biggest value for all the composites. The *K*, $t_{1/2}$ (half-life) values and synergistic factors of N-$K_2Ti_4O_9$, UiO-66 and the composites are summarized in Table 2.

Table 2. Photocatalytic degradation kinetic values for RhB

Sample	$K \times 10^2/h^{-1}$	$t_{1/2}$/h	Synergistic Factor
N-$K_2Ti_4O_9$	3.51	19.8	/
UiO-66	12.0	5.77	/
N-$K_2Ti_4O_9$/$ZrCl_4$(1:9)	9.86	7.03	1.20
N-$K_2Ti_4O_9$/$ZrCl_4$(2:8)	14.5	4.75	2.12
N-$K_2Ti_4O_9$/$ZrCl_4$(3:7)	29.5	2.35	4.90
N-$K_2Ti_4O_9$/$ZrCl_4$(4:6)	25.7	2.70	4.43
N-$K_2Ti_4O_9$/$ZrCl_4$(5:5)	22.4	3.09	4.22

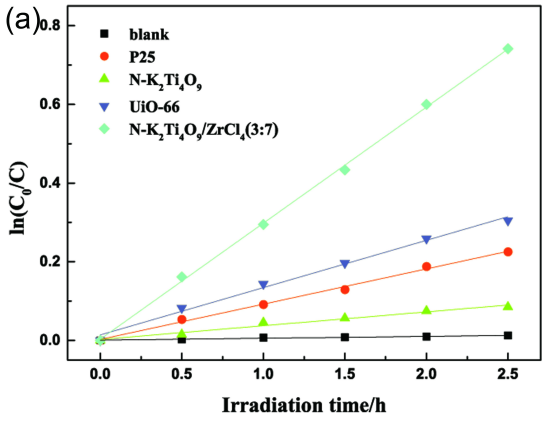

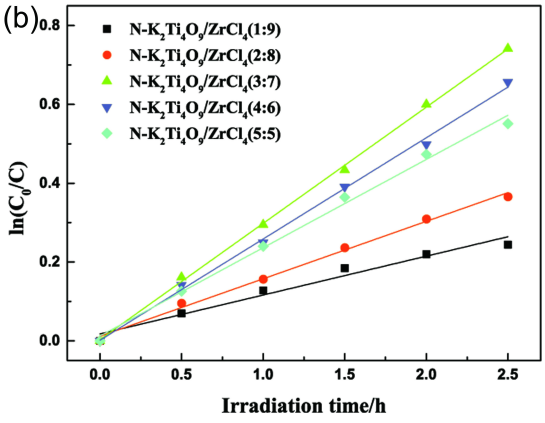

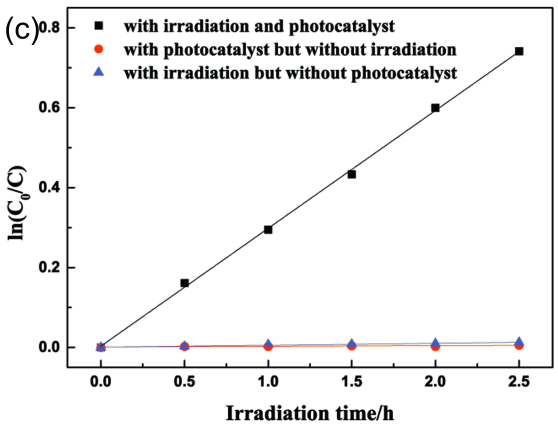

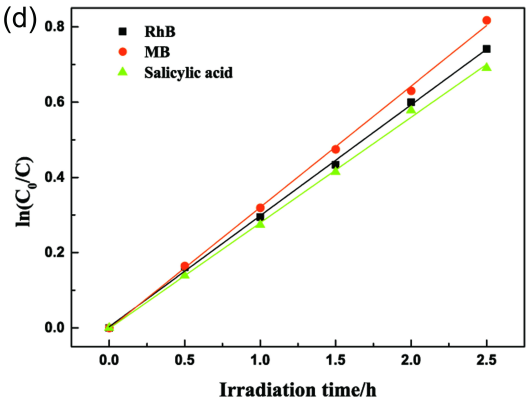

Figure 5. (a)Kinetics of RhB photodegradation on blank, P25, UiO-66, N-$K_2Ti_4O_9$ and N-$K_2Ti_4O_9$/$ZrCl_4$(3:7); (b) Kinetics of RhB photodegradation on the composites with different molar ratios of N-$K_2Ti_4O_9$ to $ZrCl_4$; (c) Kinetics of different pollutants photodegradation on N-$K_2Ti_4O_9$/$ZrCl_4$(3:7); (d) Kinetics of RhB photodegradation on N-$K_2Ti_4O_9$/$ZrCl_4$(3:7) with or without irradiaton

In order to confirm that RhB was not photodegraded by itself, a control experiment was carried out, and the result shows that there is no noticeable change in RhB concentration after 2.5h stirring under visible light irradiation without photocatalyst (Figure 5c). Another control experiment also shows that RhB was not photodegraded on photocatalyst after 2.5h without visible light irradiation (Figure 5d). These phenomena of the photobleaching can only happen under the existence of both irradiation and photocatalyst, and isn't the result of the autocatalysis.

However, RhB can have charge-transfer excitation-like transition from the HOMO to the LUMO by absorbing visible light. We choose two organic pollutants, methylene blue (MB) and salicylic acid that can and can't be excited by visible light respectively, to determine the effect of photosensitization on photocatalytic process. Figure 5d shows that the photodegradation activities of MB and salicylic acid are both close to that of RhB, which means that photosensitization is not the main factor in photocatalysis.

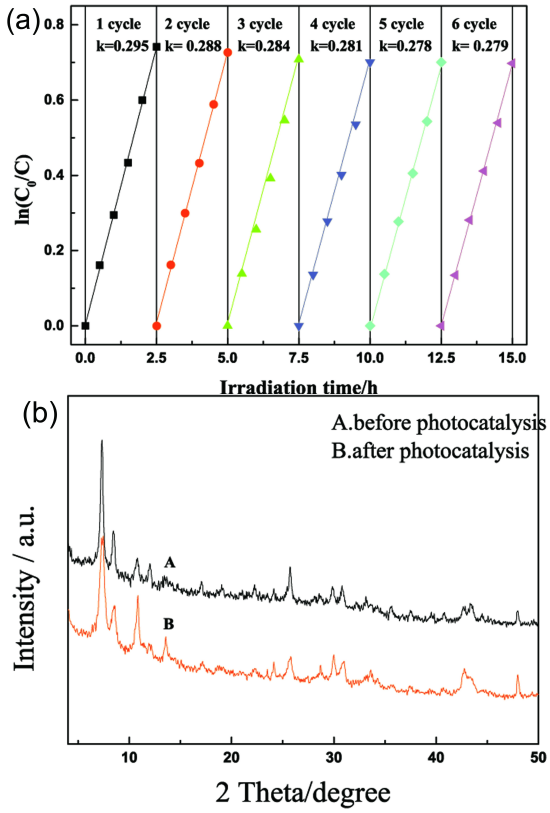

Figure 6. (a) Kinetics and rate constant of RhB photodegradation on the recycled N-$K_2Ti_4O_9$/$ZrCl_4$(3:7); (b) XRD patterns of N-$K_2Ti_4O_9$/$ZrCl_4$(3:7) before and after photocatalysis

The regeneration of the photocatalyst is one of the important steps for practical applications. The stability of N-$K_2Ti_4O_9$/$ZrCl_4$(3:7) was investigated, and after each photodegradation, it was separated from solution by centrifuge, and can be reused without considerable amount of mass loss. As shown in Figure 6a, after six cycles, the *K* value stabilized at about 0.278 h^{-1}, which is 94.24% of the first cycle.The good structural stability of N-$K_2Ti_4O_9$/$ZrCl_4$(3:7) was further verified by XRD, as shown in Figure 6b.

3.4. Photodegradation Mechanism of RhB

We had investigated the effects of both adsorption capacity and the separation efficiency of photogenerated electron-hole pairs on the photocatalytic activities of N-$K_2Ti_4O_9$/UiO-66 composites.

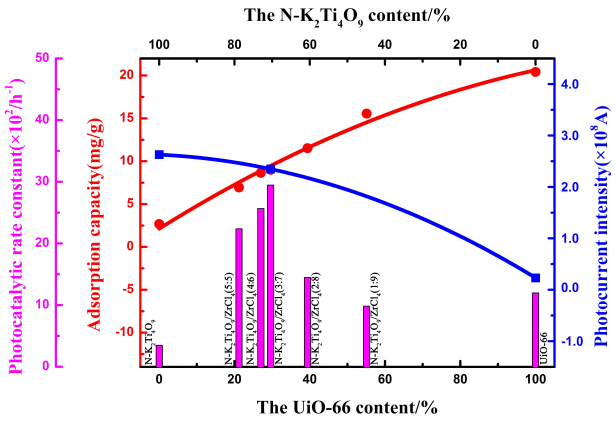

Figure 7. The dependence of photocatalytic rate constant, adsorption capacity and photocurrent intensity on the UiO-66 content of N-$K_2Ti_4O_9$, UiO-66 and the N-$K_2Ti_4O_9$/UiO-66 composites.

As shown in Figure 7, the variation of adsorption capacity is contrary to that of photocurrent intensity. With the UiO-66 content increasing in the range of 0%-29.6%, the separation efficiency of photogenerated electron-hole pairs of composites decreases a little, but the adsorption activity of composites increases a lot. These lead to great enhancement of the photocatalytic activity [36, 37]. However, when the UiO-66 content continues to increase, the photocatalytic activity quickly decreases. It is interesting that when the UiO-66 content increases to 100%, the photocatalytic rate constant increases a little.

In general, the composites display poor photocatalytic activity, when they have low adsorption capacity or low separation efficiency of photogenerated electron-hole pairs. These indicate that both adsorption capacity [38, 39] and separation efficiency of photogenerated electron-hole pairs are the key factors to determine the photocatalyst activity. When the UiO-66 content in composite is 29.6%, the synergistic effect of the two key factors achieves the optimal state, therefore, the composite shows the best photocatalytic activity.

Based on the calculated band-gaps and valence bands of UiO-66 and N-$K_2Ti_4O_9$, the mechanism of synergistic effect can be drawn in Figure 8. As RhB has charge-transfer excitation-like transition from the HOMO to the LUMO, its photogenerated electrons can transfer to the conduction band (CB) of N-$K_2Ti_4O_9$ and UiO-66. Meanwhile, the valence band (VB) holes can transfer from the VB of N-$K_2Ti_4O_9$ to the VB of UiO-66 after N-$K_2Ti_4O_9$ was excited by visible light. The impurity level (IL) is introduced from nitrogen doping to facilitate absorption of visible light [40]. These are advantageous for the separation of photogenerated electron-hole pairs and their transferring through the interface of N-$K_2Ti_4O_9$, UiO-66 and RhB, which can increase the photocatalytic activity [41].

Then, dissolved O_2 captures the photogenerated electron at CB of UiO-66 and N-$K_2Ti_4O_9$ to yield first the superoxide radical anion, $O_2^{\bullet-}$, and then the HOO• radical upon protonation. The •OH radical can be produced from the trapped electron after formation of the HOO• radical by equations (5) and (6) [42].

$$HOO\bullet + H^+ + e^- \rightarrow H_2O_2 \quad \text{..... (5)}$$

$$H_2O_2 + e^- \rightarrow \bullet OH + OH^- \quad \text{..... (6)}$$

The active oxygen species $O_2^{\bullet-}$, HOO• and •OH have been involved in the degradation of RhB. Meanwhile, the photogenerated holes in the VB of UiO-66 can directly destroy the adsorbed RhB or react with H_2O to yield •OH radicals.

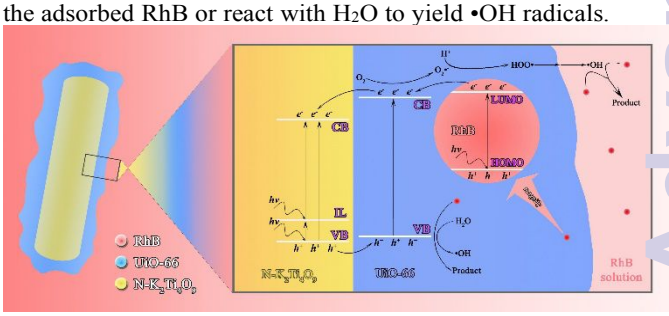

Figure 8. Mechanism diagram of the RhB photodegradation

In summary, a possible mechanism of photocatalysis with N-$K_2Ti_4O_9$/UiO-66 composites under visible light irradiation is proposed (Figure 8). UiO-66 as a shell around the N-$K_2Ti_4O_9$ core can enhance the adsorption of RhB from solution. Then the excited state electrons in LUMO of RhB can readily migrate to CB of UiO-66 and N-$K_2Ti_4O_9$, and react with dissolved O_2 to

yield active oxygen species, which will degrade RhB. Meanwhile, N-$K_2Ti_4O_9$ absorbs visible light to produce photogenerated electron-hole pairs, and its holes can migrate easily to the VB of UiO-66, and destroy the adsorbed RhB or react with H_2O to yielded •OH radicals.

Conclusions

In conclusion, the N-$K_2Ti_4O_9$/UiO-66 composites were synthesized by a facile solvothermal method, and possess a hierarchical core-shell structure with UiO-66 forming the shell around the N-$K_2Ti_4O_9$ core, which is beneficial for promoting the photodegradation of RhB. The synergistic effect of photocatalysis is due to big adsorption capacity of UiO-66 and high separation efficiency of photogenerated electron-hole pairs at interfaces of N-$K_2Ti_4O_9$ and UiO-66. In particular, N-$K_2Ti_4O_9$/$ZrCl_4$(3:7) exhibits the best photocatalytic activity among the composites, and the synergistic factor is 4.90.

Acknowledgements

This work was supported by the Anhui Provincial Natural Science Foundation (NO.1508085MB28 and NO.1308085MB21) and the National Natural Science Foundation of China (No. 51372062).

Notes and references

1 A. Dolbecq, P. Mialane, B. Keita, L. Nadjo, J. Mater. Chem. 2012, 22, 24509.
2 A. Kubacka, M. Fernández-García, G. Colón, Chem. Rev. 2012, 112, 1555.
3 W. Q. Fan, Q. H. Zhang, Y. Wang, Phys. Chem. Chem. Phys. 2013, 15, 2632.
4 X. B. Chen, S. H. Shen, L. J. Guo, S. S. Mao, Chem. Rev. 2010, 110, 6503.
5 J. S. Wang, H. Li, H. Y. Li, S. Yin, T. Sato, Solid State Sci. 2009, 11, 988.
6 P. Romero-Gómez, S. Hamad, J. C. González, A. Barranco, J. P. Espinós, J. Cotrino, A. R. González-Elipe, J. Phys. Chem. C 2010, 114, 22546.
7 Y. J. Hwang, A. Boukai, P. D. Yang, Nano Lett. 2009, 9, 410.
8 H. L. Li, M. Eddaoudi, M. O'Keeffe, O. M. Yaghi, Nature 1999, 402, 276.
9 O. M. Yaghi, M. O'Keeffe, N. W. Ockwig, H. K. Chae, M. Eddaoudi, J. Kim, Nature 2003, 423, 705.
10 S. Kitagawa, R. Kitaura, S. I. Noro, Angew. Chem. Int. Ed. 2004, 43, 2334.
11 S. Kitagawa, R. Matsuda, Coordin. Chem. Rev.2007, 251, 2490.
12 G. Fe´rey, Chem. Soc. Rev. 2008, 37, 191.
13 S. Hasegawa, S. Horike, R. Matsuda, S. Furukawa, K. Mochizuki, Y. Kinoshita, S. Kitagawa, J. Am. Chem. Soc. 2007,129, 2607.
14 M. Eddaoudi, J. Kim, N. Rosi, D. Vodak, J. Wachter, M. OÕKeeffe, O. M. Yaghi, Science 2002, 295, 469.
15 N. L. Rosi, J. Eckert, M. Eddaoudi, D. T. Vodak, J. Kim, M. O'Keeffe, O. M. Yaghi, Science 2003, 300, 1127.
16 M. Latroche, S. Surblé, C. Serre, C. Mellot-Draznieks, P. L. Llewellyn, J. H. Lee, J. S. Chang, S. H. Jhung, G. Férey, Angew. Chem. Int. Ed. 2006, 45, 8227.
17 P. Horcajada, C. Serre, M. Vallet-Regí, M. Sebban, F. Taulelle, G. Férey, Angew. Chem. 2006, 118, 6120.
18 J. H. Cavka, S. Jakobsen, U. Olsbye, N. Guillou, C. Lamberti, S. Bordiga, K. P. Lillerud, J. Am. Chem. Soc. 2008, 130, 13850.
19 L. Valenzano, B. Civalleri, S. Chavan, S. Bordiga, M. H. Nilsen, S. Jakobsen, K. P. Lillerud, C. Lamberti, Chem. Mater. 2011, 23, 1700.
20 M. Kandiah, M. H. Nilsen, S. Usseglio, S. Jakobsen, U. Olsbye, M. Tilset, C. Larabi, E. A. Quadrelli, F. Bonino, K. P. Lillerud, Chem. Mater. 2010, 22, 6632.
21 M. Kandiah, S. Usseglio, S. Svelle, U. Olsbye, K. P. Lillerud, M. Tilset, J. Mater. Chem. 2010, 20, 9848.
22 C. G. Silva, I. Luz, F. X. LlabrésiXamena, A. Corma, H. García, Chem.-Eur. J. 2010, 16, 11133.
23 M. R. Allen, A. Thibert, E. M. Sabio, N. D. Browning, D. S Larsen, F. E. Osterloh, Chem. Mater. 2010, 22, 1220.
24 D. Mitoraj, H. Kisch, Angew. Chem. Int. Edit.2008,47, 9975.
25 A. Schaate, P. Roy, A. Godt, J. Lippke, F. Waltz, M. Wiebcke, P. Behrens, Chem.-Eur. J. 2011, 17, 6643.
26 S. J. Gregg, K. S. Sing, Academic Press: New York, 1967.
27 Z. G. Xiong, X. S. Zhao, J. Am. Chem. Soc. 2012, 134, 575
28 D. F. Wang, J. W. Tang, Z. G. Zou, J. H. Ye, Chem. Mater. 2005, 17, 5177.
29 M. A. Butler, J. Appl. Phys.1914, 48, 1914.
30 X. B. Chen, L. Liu, P. Y. Yu, S. S. Mao, Science 2011, 331, 746.
31 P. Xiong, Q. Chen, M. Y. He, X. Q. Sun, X.Wang, J. Mater. Chem.2012, 22, 17485.
32 P. Xiong, L. J. Wang, X. Q. Sun, B. H. Xu, X. Wang, Ind. Eng. Chem. Res. 2013, 52, 10105.
33 F. B. Li, X. Z. Li, Appl. Catal. A 2002,228, 15.
34 J. G. Yu, H. G. Yu, B. Cheng, X. J. Zhao, J. C. Yu, W. K. Ho, J. Phys. Chem. B 2003, 107, 13871.
35 Q. Chen, Q. Q. He, M. M. Lv, X. T. Liu, J. Wang, J. P. Lv, Appl. Surf. Sci. 2014, 311, 230.
36 Y. J. Wang, R. Shi, J. Lin, Y. F. Zhu, Energy Environ. Sci. 2011, 4, 2922.
37 Y. B. Xie, C. W. Yuan, X. Z. Li, Mater Sci Eng B. 2005, 117, 325-333.
38 T. L. Xu, Y. Cai, K. E. O'Shea, Environ. Sci. Technol. 2007, 41, 5471.
39 C. S. Pan, J. Xu, Y. J. Wang, D. Li, Y. F. Zhu, Adv. Funct. Mater.2012, 22, 1518.
40 L. Xu, E. M. P. Steinmiller, S. E. Skrabalak, J. Phys. Chem. C 2012, 116, 871.
41 W. J. Li, D. Z. Li, S. G. Meng, W. Chen, X. Z. Fu, Y. Shao, Environ. Sci. Technol. 2011, 45, 2987.
42 T. X. Wu, G. M. Liu, J. C. Zhao, J. Phys. Chem. B 1998, 102, 5845.